The Atmospheric Radiation Measurement Program Cloud Radars: Operational Modes

EUGENE E. CLOTHIAUX,* KENNETH P. MORAN,+ BROOKS E. MARTNER,+ THOMAS P. ACKERMAN,*
GERALD G. MACE,# TANEIL UTTAL,+ JAMES H. MATHER,* KEVIN B. WIDENER,@
MARK A. MILLER,& AND DANIEL J. RODRIGUEZ**

* *Department of Meteorology, The Pennsylvania State University, University Park, Pennsylvania*
+ *NOAA Environmental Technology Laboratory, Boulder, Colorado*
# *Department of Meteorology, University of Utah, Salt Lake City, Utah*
@ *Batelle, Pacific Northwest National Laboratory, Richland, Washington*
& *Division of Applied Science, Brookhaven National Laboratory, Upton, New York*
** *Atmospheric Science Division, Lawrence Livermore National Laboratory, Livermore, California*

(Manuscript received 11 March 1998, in final form 24 August 1998)

ABSTRACT

During the past decade, the U.S. Department of Energy (DOE), through the Atmospheric Radiation Measurement (ARM) Program, has supported the development of several millimeter-wavelength radars for the study of clouds. This effort has culminated in the development and construction of a 35-GHz radar system by the Environmental Technology Laboratory (ETL) of the National Oceanic and Atmospheric Administration (NOAA). Radar systems based on the NOAA ETL design are now operating at the DOE ARM Southern Great Plains central facility in central Oklahoma and the DOE ARM North Slope of Alaska site near Barrow, Alaska. Operational systems are expected to come online within the next year at the DOE ARM tropical western Pacific sites located at Manus, Papua New Guinea, and Nauru. In order for these radars to detect the full range of atmospheric hydrometeors, specific modes of operation must be implemented on them that are tuned to accurately detect the reflectivities of specific types of hydrometeors. The set of four operational modes that are currently in use on these radars are presented and discussed. The characteristics of the data produced by these modes of operation are also presented in order to illustrate the nature of the cloud products that are, and will be, derived from them on a continuous basis.

1. Introduction

To fully understand the radiative impact of clouds on the climate system, both the macrophysical (i.e., horizontal and vertical distributions) and microphysical properties (i.e., particle shapes, sizes, and number concentrations) of clouds must be known. Whereas the horizontal distribution of clouds over the earth is characterized currently by passive radiometry from satellites, mapping the vertical distribution of clouds is achieved best using lidars and radars. Lidars are able to detect all types of cloud particles in circumstances in which the lidar beam is able to penetrate to the location of the cloud particles. However, complete extinction of a lidar beam during heavy overcast, or a period with multiple cloud layers, is not uncommon. Millimeter-wavelength radar observations are a natural complement to collocated lidar observations since radars operating at millimeter wavelengths can detect most cloud particles, and a millimeter-wavelength radar beam generally penetrates all cloud types except those that occur during periods of heavy rain. Radars operating at 35- and 94-GHz are used the most since the attenuation of the beam as a result of absorption by oxygen and water vapor is at a local minimum near these frequencies.

To provide the capability of mapping the vertical distribution of clouds in a few different climate regimes, the U.S. Department of Energy (DOE) Atmospheric Radiation Measurement (ARM) Program contracted the Environmental Technology Laboratory (ETL) of the National Oceanic and Atmospheric Administration (NOAA) to build a number of millimeter-wavelength radars. A detailed description of these completely automated, continuously operating, vertically pointing Doppler radars is given by Moran et al. (1998). They are millimeter-wave systems that operate at 34.86 GHz (8.7-mm wavelength). In the ARM nomenclature they are referred to as millimeter-wavelength cloud radars (MMCR), and they are being installed at the ARM Cloud and Radiation Testbed (CART) sites. The first unit began operation at the Southern Great Plains (SGP) CART site near Lamont, Oklahoma, in November 1996.

Corresponding author address: Eugene E. Clothiaux, Department of Meteorology, 503 Walker Building, The Pennsylvania State University, University Park, PA 16802.
E-mail: cloth@essc.psu.edu

The second unit began operation at the North Slope of Alaska (NSA) CART site near Barrow, Alaska, in March 1998. Two additional MMCRs will begin operation at the tropical western Pacific (TWP) CART sites on Manus, Papua New Guinea, and Nauru within the next year. The MMCRs are expected to continue operation at the CART sites for approximately 10 years.

The profiles of hydrometeor reflectivities and vertical velocities produced by the ARM MMCRs are important for successful realization of three ARM goals, which are to better understand the impact of clouds on the radiation budget, improve the parameterizations of radiative transfer and clouds in numerical weather prediction and global climate models, and validate satellite retrievals. Currently, algorithms are being developed that will detect significant returns in the MMCR data and thereby ascertain the distribution of the hydrometeors in the vertical column above the ARM sites. ARM retrieval algorithms, which combine cloud observations by the MMCR with data from nearby CART radiometers and other remote sensors, will provide estimates of the microphysical properties of the hydrometeors in the clouds overhead. Long-term records of the microphysical and macrophysical cloud properties, together with the extensive CART monitoring of radiometric fluxes at the ground, will allow the radiative impacts of clouds on climate to be investigated with unprecedented detail. The data will be used to test cloud model parameterizations and to validate cloud ensemble model simulations. They are also expected to be useful for evaluating retrievals of cloud properties from satellites, such as those of the National Aeronautics and Space Administration's Earth Observing System (EOS) platform.

The MMCR radars must be capable of detecting nearly all radiatively important clouds over the CART sites, including multiple layers of thin, weakly reflecting clouds. Furthermore, the measured reflectivities, upon which the microphysical retrievals depend, must be suitably accurate. The cloud detection requirement suggests that an MMCR must be able to detect clouds ranging from thin stratus and cirrus to clouds that produce drizzle. This represents a dynamic range of approximately -50 dBZ to $+20$ dBZ, for the measurement of the radar reflectivity factor Z. For hydrometeors that are small compared with the radar wavelength, Z, in units of mm^6 m^{-3}, is defined by the integral $\int_0^\infty N(D)D^6\,dD$, where D [mm] is the particle diameter and $N(D)$ [m^{-3} mm^{-1}] is the particle number density distribution. The transform $10\log_{10}(Z)$ casts Z into units of dBZ.

Detection of cloud reflectivities less than about -30 dBZ requires special radar techniques, even for millimeter-wave systems. The MMCR design addresses this issue by allowing for different operational modes of the radar, which can be cycled through repetitively. Some modes use pulse compression techniques with long pulses to boost radar sensitivity, allowing for detection of weakly reflecting clouds, while other modes use conventional short pulses. Each mode involves trade-offs among sensitivity, spatial resolution, temporal resolution, velocity aliasing, range aliasing, and range sidelobe artifacts. Considered together, data from the different operating modes can be combined to yield a comprehensive and accurate depiction of most of the clouds in the vertical column above the radar.

TABLE 1. Dependencies between the operational parameters of the ARM MMCRs. All variables are defined in the text except the radar wavelength represented by the variable λ.

Radar parameter relationship
$R_{\min} = R_{\text{deadtime}} + N_{\text{bits}}\Delta R$
$R_{\max} = R_{\text{deadtime}} + (N_{\text{vol}} - 1)R_{\text{space}}$
$R_u = (c\tau_{\text{ipp}})/2$
$\Delta R = (c\tau_{\text{pw}})/2$
$V_u = \lambda/(4\tau_{\text{ipp}}N_{\text{coh}})$
$\Delta V_u = (2V_u)/N_{\text{fft}}$
$T_s \propto N_{\text{vol}}$, N_{fft}, N_{spec}, 1/processor speed
Radar sensitivity $\propto \tau_{\text{pw}}$, N_{bits}
Noise fluctuations $\propto 1/N_{\text{coh}}$, $1/\sqrt{N_{\text{spec}}}$

2. Initial operational parameters of the ARM SGP radar

The functionality of the ARM MMCRs is a consequence both of the hardware that is used to build them and of the control parameters that are used to run them. The hardware features of the radar, especially its operating wavelength of approximately 8.6 mm, result from an attempt to maximize sensitivity to cloud particles and at the same time reduce the effect of atmospheric attenuation on the radar beam. For a given choice of radar hardware, the sensitivity of the radar to cloud particles can be enhanced through the choice of operational parameters that are used to run it. The primary parameters in this regard are 1) the number of range sample volumes (N_{vol}), 2) the range sample volume spacing (R_{space}), 3) the pulse width (τ_{pw}), 4) the interpulse period (τ_{ipp}), 5) the number of coded bits (N_{bits}), 6) the number of coherent averages (N_{coh}), 7) the number of spectra averaged (N_{spec}), 8) the number of fast Fourier transform (FFT) points (N_{fft}), and 9) the radar receiver deadtime (τ_{deadtime})—a short period of time during and following the pulse transmission process when the radar receiver is turned off to ensure that no significant amount of transmitter pulse power is directly reflected into the radar receiver. Once these operational parameters are set, other parameters follow as a consequence, including 1) the minimum range $R_{\min}$ of useful data, which is related to the deadtime range $R_{\text{deadtime}} = c\tau_{\text{deadtime}}$ (c is the speed of light) and the number of coded bits; 2) the maximum range $R_{\max}$ from which data are collected; 3) the unambiguous range R_u; 4) the range resolution ΔR; 5) the unambiguous velocity V_u; 6) the velocity resolution ΔV_u; 7) the sampling interval T_s; 8) the radar sensitivity; and 9) the receiver noise fluctuations (Table 1). Moran et al. (1998) describe many aspects of these parameters, and Battan (1973), Doviak

TABLE 2. Operational parameters for the ARM SGP MMCR during Apr 1997.

Mode	SGP			
	4	3	2	1
Number of range volumes (N_{vol})	220	167	167	220
Range volume spacing (R_{space}, m)	45	90	90	45
Pulse width (τ_{pw}, ns)	300	600	600	300
Interpulse period (τ_{ipp}, μs)	72	106	126	82
Number coded bits (N_{bits})	0	0	32	32
Number coherent averages (N_{coh})	4	6	6	8
Number spectra averaged (N_{spec})	37	60	21	16
Number FFT points (N_{fft})	64	64	64	64
Minimum range (R_{min}, m)	105	105	2985	1545
Maximum range (R_{max}, m)	9960	15 045	15 045	9960
Unambiguous range (R_u, m)	10 800	15 900	18 900	12 300
Range volume resolution (ΔR, m)	45	90	90	45
Unambiguous velocity (V_u, m s^{-1})	7.46	3.38	2.84	3.28
Velocity resolution (ΔV_u, m s^{-1})	0.23	0.11	0.09	0.10
Time resolution (T_s, s)	9.0	9.0	9.0	9.0
Minimum detected signal (dBm)	−132	−132	−132	−129
Estimated sensitivity (5 km, dBZ_e)	−30	−34	−49	−47

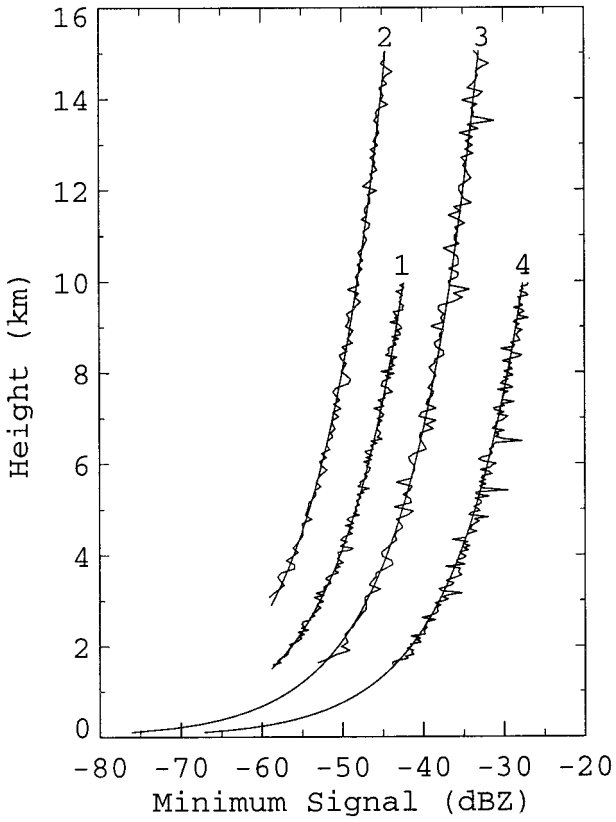

FIG. 1. Minimum detectable reflectivities for the four modes in operation on the ARM SGP MMCR during Apr 1997. The jagged solid curves represent the mean plus one standard deviation for data that was collected during a 90-min clear-sky period on 14 Apr 1997. The smooth solid lines are generated from a fit of the radar equation to the clear-sky data and span the height range for which the data from the mode are usable.

and Zrnic (1984, 1993), Sauvageot (1992), Skolnik (1980, 1990) and Ulaby et al. (1982) provide detailed discussions on operational aspects of radar.

The starting point for the current analysis is the four operational modes presented by Moran et al. (1998) for the ARM SGP MMCR. The characteristics of these four modes are presented in Table 2 for completeness. The ARM SGP MMCR was operated from 7 November 1996 through 15 September 1997 with modes comparable to these four. The sensitivity of each mode as a function of range is illustrated in Fig. 1. To generate the results presented in Fig. 1, the 9-s interval radar reflectivities for each mode within each range resolution volume were first averaged over a 90-min block of time during clear-sky conditions. The standard deviations of reflectivity with respect to the 90-min mean reflectivities were then computed. To obtain an estimate of the minimum detectable signal for range resolution volumes above approximately 2 km, the mean and standard deviation of the reflectivities for each resolution volume were added together. The results of this process are the jagged solid lines in Fig. 1. Since no clouds were present during the averaging interval, the variability in the estimate of the minimum detectable signal with height is the result of receiver noise, at least for the profiles above 2 km that are illustrated in Fig. 1. Below 2 km, contributions to the radar return powers from particulate matter, such as insects, are important. (The variability in the receiver noise and the contribution of clutter to the radar return powers are what make identifying significant but small cloud power returns difficult.) Best-fit curves of the radar equation $P_{min}(r) = R_c \eta_{min}(r) r^{-2}$—where $P_{min}(r)$ is the minimum detectable power in the radar receiver, R_c is the radar constant, and $\eta_{min}(r)$ is the minimum detectable reflectivity at range r—to the data from heights above 2 km were then computed in order to extend the minimum detectable signals to all heights for which each mode is used.

The four modes in this initial set fall into two groups. The first group composed of modes 1 and 2 is characterized by 32-bit complementary binary phase coding for enhanced sensitivity (Schmidt et al. 1979), while the second group composed of modes 3 and 4 is characterized by a transmitted pulse with no phase coding. The most significant difference between the two modes within a group is the range resolution, one mode having a resolution of 45 m and the other having a resolution of 90 m. The high-resolution modes (i.e., modes 1 and 4) have a maximum range R_{max} of approximately 10 km, while the low-resolution modes reach altitudes of 15 km. The number N_{vol} of sample volumes, and hence R_{max}, in a mode of operation is limited by the radar processor. The high-resolution modes are less sensitive than their low-resolution counterparts by approximately 5 and 9 dB for the first and second groups, respectively. Although data are collected from 105 m to R_{max} for both of the phase-coded modes in the first group, the stated values of R_{min} in Table 2 for modes 1 and 2 are 1545 and 2985 m, respectively, reflecting the artifacts in the reflectivity data as a result of partial decoding between 105 m and a distance of $N_{bits}\Delta R$ above this height.

From the perspective of detection, modes 2 and 3 in this initial set of four are the most useful. In fact, mode 2 has a minimum detectable reflectivity below -50 dBZ up to a height of approximately 8 km, and at 14 km the minimum detectable reflectivity is -45 dBZ. This mode, therefore, approaches the scientific requirement of being able to detect cloud particles with reflectivities as low as -50 dBZ at any altitude within the troposphere above 3 km. However, a problem with mode 2 is the range sidelobe artifacts that result from phase coding (Wakasugi and Fukao 1985; Skolnik 1990; Moran et al. 1998). Radar sample volumes within 2880 m ($=N_{bits}\Delta R$) of sample volumes containing particles with large fall velocities and large reflectivities can appear to generate significant power returns when in fact they do not. In and around the vicinity of radar sample volumes that lead to range sidelobe artifacts, mode 3 is a natural complement to mode 2, as it readily can detect rapidly moving large particles that lead to problems in mode 2. Importantly, mode 3 also has a minimum detectable reflectivity below -50 dBZ at heights under 2 km.

An important parameter in all four of the modes is the number N_{coh} of coherent integrations. Since N_{coh} is greater than 1 for all modes, attenuation of the return power through the coherent integration circuitry is not negligible as the particle velocities with respect to the radar approach the radar Nyquist velocity (Schmidt et al. 1979). The power transfer function through the coherent integration device as a function of velocity for the four modes is shown in Fig. 2. As this figure illustrates, the reflectivity of any collection of hydrometeors with fall speeds exceeding approximately 3 m s^{-1} in a radar sample volume above 10 km will be underestimated when using the reflectivity estimates produced by the four modes. A similar situation occurs for particles in radar sample volumes below 10 km if the particle velocities exceed 7 m s^{-1}. If accurate estimates of particle reflectivities, apart from the effects of atmospheric attenuation, are to be made at all heights for all times, then an adjustment to one of the modes must be made to alleviate the problems associated with coherent integration.

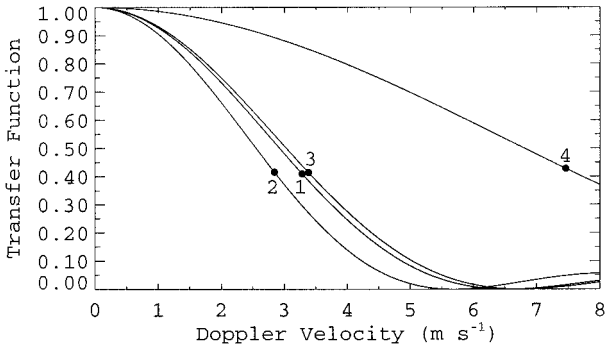

FIG. 2. The power transfer function through the coherent integration circuitry. The numbers identify the transfer function for each mode, and the Nyquist velocity for each mode is indicated by the filled circles.

After visually inspecting several months of radar returns, we noticed that the two modes with complementary binary phase coding sometimes appeared to detect boundary layer clouds that were missed by the uncoded modes. However, the partial decoding of the coded modes in the vicinity of the boundary layer clouds complicated extraction of the exact location and reflectivity of these clouds. These results indicated the need for a mode with better sensitivity than modes 3 and 4 in the boundary layer. The set of four modes currently running on the ARM SGP MMCR, which we now discuss, attempts to correct for the coherent integration and boundary layer cloud detection problems just discussed while preserving the sensitivity and complementary nature of modes 2 and 3.

3. Current operational parameters of the ARM SGP radar

The primary difference between the initial modes 1 and 2, as well as the initial modes 3 and 4, is spatial resolution and sensitivity. For weakly reflecting middle- and upper-level tropospheric clouds, mode 2 is more valuable than mode 1 simply because mode 2 detects more of these clouds than mode 1. We concluded, therefore, that the higher spatial resolution of mode 1 was not an important attribute in the middle and upper troposphere. Consequently, mode 1 was adjusted in an attempt to maximize its sensitivity to boundary layer clouds. Although an uncoded mode would be preferable for remotely sensing boundary layer clouds, the requisite sensitivity for detecting the boundary layer clouds previously identified in the phase-coded modes, but not the uncoded modes, could not be attained without phase coding. Therefore, the number N_{bits} of coded bits was

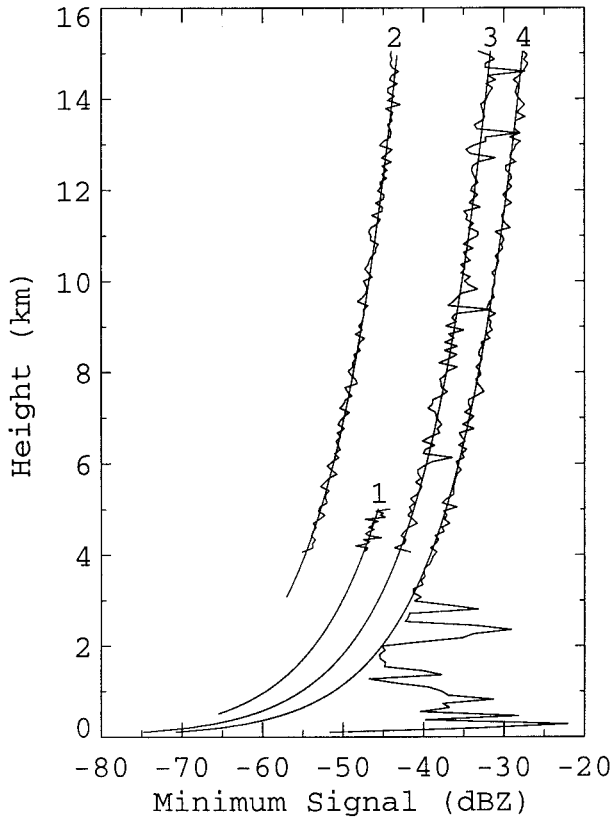

FIG. 3. Same as for Fig. 1 except for the four modes in continuous operation since 16 Sep 1997. Note that the large reflectivities in the SGP MMCR mode 4 plot below approximately 3 km are due to insects, dust, etc., near the surface.

set to 8, down from 32. In order to keep the partial decoding close to the surface, the range resolution ΔR was kept at 45 m. To further enhance sensitivity of mode 1 beyond phase coding, the duty cycle was increased by decreasing the interpulse period τ_{ipp} from 82 to 68 μs. The change in τ_{ipp} lowered the unambiguous range from 12.3 to 10.2 km, while allowing us to increase the number of coherent averages from 8 to 10 with almost no change in the Nyquist velocity. To perform as much incoherent averaging as possible on the radar returns from the lower troposphere, only the radar sample volumes up to 5010 m are processed, thereby saving the time that would be required to process the radar data acquired from higher altitudes. Consequently, the number of spectra averaged increased from 16 to 64, while the sample time interval T_s remained at 9 s. The end result was that mode 1 retained much of its original sensitivity (Fig. 3), while R_{min} dropped from 1500 m to 465 m (Table 3). In its current configuration, mode 1 has perhaps the highest sensitivity to nonprecipitating, weakly reflecting boundary layer clouds that is possible with the current MMCR hardware.

The same considerations that applied to modes 1 and 2 also apply to modes 3 and 4: in the upper troposphere

Table 3. Current operational parameters for the MMCRs at the ARM SGP and NSA sites, and planned operational parameters for the ARM TWP MMCRs.

	SGP				TWP				NSA			
Mode	4	3	2	1	4	3	2	1	4	3	2	1
Number of range volumes (N_{vol})	167	167	167	110	226	226	226	134	221	149	149	135
Range volume spacing (R_{space}, m)	90	90	90	45	90	90	90	45	45	90	90	45
Pulse width (τ_{pw}, ns)	600	600	600	300	600	600	600	300	300	600	600	300
Interpulse period (τ_{ipp}, μS)	106	106	126	68	142	142	160	90	90	96	115	68
Number coded bits (N_{bits})	0	0	32	8	0	0	32	8	0	0	32	8
Number coherent averages (N_{coh})	1	6	6	10	1	5	4	8	2	7	6	10
Number spectra averaged (N_{spec})	29	60	21	64	20	44	16	50	20	70	23	50
Number FFT points (N_{fft})	128	64	64	64	128	64	64	64	128	64	64	64
Minimum range (R_{min}, m)	105	105	2985	465	105	105	2985	465	105	105	2985	465
Maximum range (R_{max}, m)	15 045	15 045	15 045	5010	20 355	20 355	20 355	6090	10 005	13 425	13 425	6135
Unambiguous range (R_u, m)	15 900	15 900	18 900	10 200	21 300	21 300	24 000	13 500	13 500	14 400	17 250	10 200
Range volume resolution (ΔR, m)	90	90	90	45	90	90	90	45	45	90	90	45
Unambiguous velocity (V_u, m s^{-1})	20.28	3.38	2.84	3.16	15.14	3.03	3.36	2.99	11.94	3.20	3.12	3.16
Velocity resolution (ΔV_u, m s^{-1})	0.32	0.11	0.09	0.10	0.24	0.09	0.11	0.09	0.19	0.10	0.10	0.10
Time resolution (T_s, s)	9.0	8.5	8.7	9.0	9.0	8.6	9.0	8.5	9.0	9.0	9.0	9.0
Minimum detected signal (dBm)	−132	−135	−133	−135	−131	−134	−131	−134	−131	−136	−133	−134
Estimated sensitivity (5 km, dBZ$_e$)	−38	−42	−54	−47	−32	−35	−48	−41	−32	−40	−51	−44

mode 3 is more valuable than mode 4 because mode 3 is a more sensitive mode. The higher spatial resolution data of mode 4 in the boundary layer is also redundant to an extent now because of the revisions made to mode 1. Furthermore, the higher sensitivity of mode 3, as compared to mode 4, makes it a more useful mode for detecting weakly reflecting boundary layer clouds. Therefore, we changed the characteristics of mode 4 from a high spatial resolution mode to one that produces accurate reflectivities, apart from atmospheric attenuation, under all conditions from the surface up to the tropopause. To this end, R_{space} and ΔR were increased from 45 to 90 m, and coherent integration was eliminated from this mode. Consequently, the transfer function for mode 4 illustrated in Fig. 2 now takes on a constant value of 1 for all Doppler velocities, and mode 4 produces reliable reflectivity and velocity estimates for rapidly falling large particles. Increasing R_{space} and ΔR to 90 m and setting N_{vol} to 167, R_{max} increased from 9960 to 15 045 m. To increase the unambiguous range R_u to a value greater than R_{max}, τ_{ipp} was set to 106 μs, up from 72 μs. With all of these changes, the unambiquous velocity V_u increased to 20.28 m s^{-1}. To improve the velocity resolution for such a large Nyquist velocity, the number N_{fft} of points per FFT was doubled to 128. The new sensitivity of mode 4 is illustrated in Fig. 3, and its operating characteristics are provided in Table 3.

The final set of four modes now running on the ARM SGP MMCR consists of the original modes 2 and 3 first presented by Moran et al. (1998), together with modes 1 and 4 that we just now discussed (Table 3). The characteristics of each mode are set to accurately determine the reflectivities of certain kinds of hydrometeors: 1) a robust mode (mode 4, Fig. 4a) that produces accurate reflectivities at all heights all of the time; 2) a general mode (mode 3, Fig. 4b) that is fairly sensitive to all cloud particles at all altitudes with no data artifacts except during heavier precipitation; 3) a cirrus mode (mode 2, Fig. 4c) that is tuned to detecting weakly reflecting mid- and higher-level clouds and 4) a boundary layer stratus mode (mode 1, Fig. 4d) that is tuned to detecting weakly reflecting lower-level clouds. When considered together, these four modes appear to provide the required sensitivity with few, if any, artifacts in the data (Fig. 4e). One exception is a result of the 64-dB dynamic range of mode 4. (The mode 4 dynamic range is the largest.) For example, when hydrometeor reflectivities approach approximately 10–15 dBZ at an altitude of 1 km, nonlinearities in the receiver dynamic range become apparent in the mode 4 reflectivities.

4. Discussion and conclusions

The set of four modes presented in Table 3 for the ARM SGP MMCR has now been in use from 16 September 1997 until the present. The four modes presented in Table 3 for the NSA and TWP MMCRs are a natural extension to the current SGP MMCR set. The NSA MMCR has been operating with the set of modes in Table 3 since being brought online on 26 March 1998, and the TWP MMCRs will use the modes in Table 3 when brought online in Nauru and Manus, Papua New Guinea, during 1998 and 1999, respectively.

To identify artifacts in the pulse-coded data produced by modes 1 and 2, we currently are using the test described by Moran et al. (1998). Let $P(n)$ represent the nonrange-corrected power that results from the nth radar sample volume of mode 4. This sample volume is flagged as possibly suffering from range sidelobe artifacts in the mode 2 data if

$$P(k) > P(n) + T$$

for any value of k that satisfies $n - 31 < k < n + 31$. A value of the threshold T that identifies most range sidelobe artifacts is 25 dB. A threshold value of 15 dB eliminates those rare artifacts that are not identified by the 25-dB value. Though this is a simple test, in practice it works quite well for the mode 2 data because the data removed by it can generally be replaced with data produced by modes 3 and 4. The one exception, however, is for weak cirrus returns that occur within approximately 3000 m of stronger cloud returns. In these situations, modes 3 and 4 may fail to detect the weak cirrus returns, while the mode 2 data may be range sidelobe contaminated. In an attempt to recover weak returns that are lost in the present processing, more sophisticated algorithms for handling range sidelobe effects are being developed at the National Oceanic and Atmospheric Administration ETL.

Importantly, both in the original set of modes presented by Moran et al. (1998) and in the final set of modes developed here, modes 1, 2, and 3 have comparable velocity resolutions. Therefore, when Doppler velocity and width data are combined from these three modes, there are no large discontinuities in the final fields. In regions in which the reflectivities and velocities are large, mode 4 data are used, which entails a loss of velocity resolution. Consequently, in some kinds of scientific studies, such as detailed time series analyses over relatively long time periods, only continuous data from a particular mode may be of use.

Each mode of the MMCRs currently has a temporal resolution of approximately 9 s. The temporal resolution can be shortened, but at the cost of lower sensitivity. The efficiency of the radar signal processor currently ranges from 4% to 31% for SGP MMCR modes 4 through 1; that is, the computers can process only a small portion of the data that the radar can generate. A new version of the radar processor is planned that will significantly improve the performance of the radar. This processor will provide two major benefits. First, coherent integration can be implemented using FFTs with more points rather than time series integration. This eliminates the spectral weighting that time series integration imposes and it increases V_u, thereby reducing the chances of folded velocity measurements. Second,

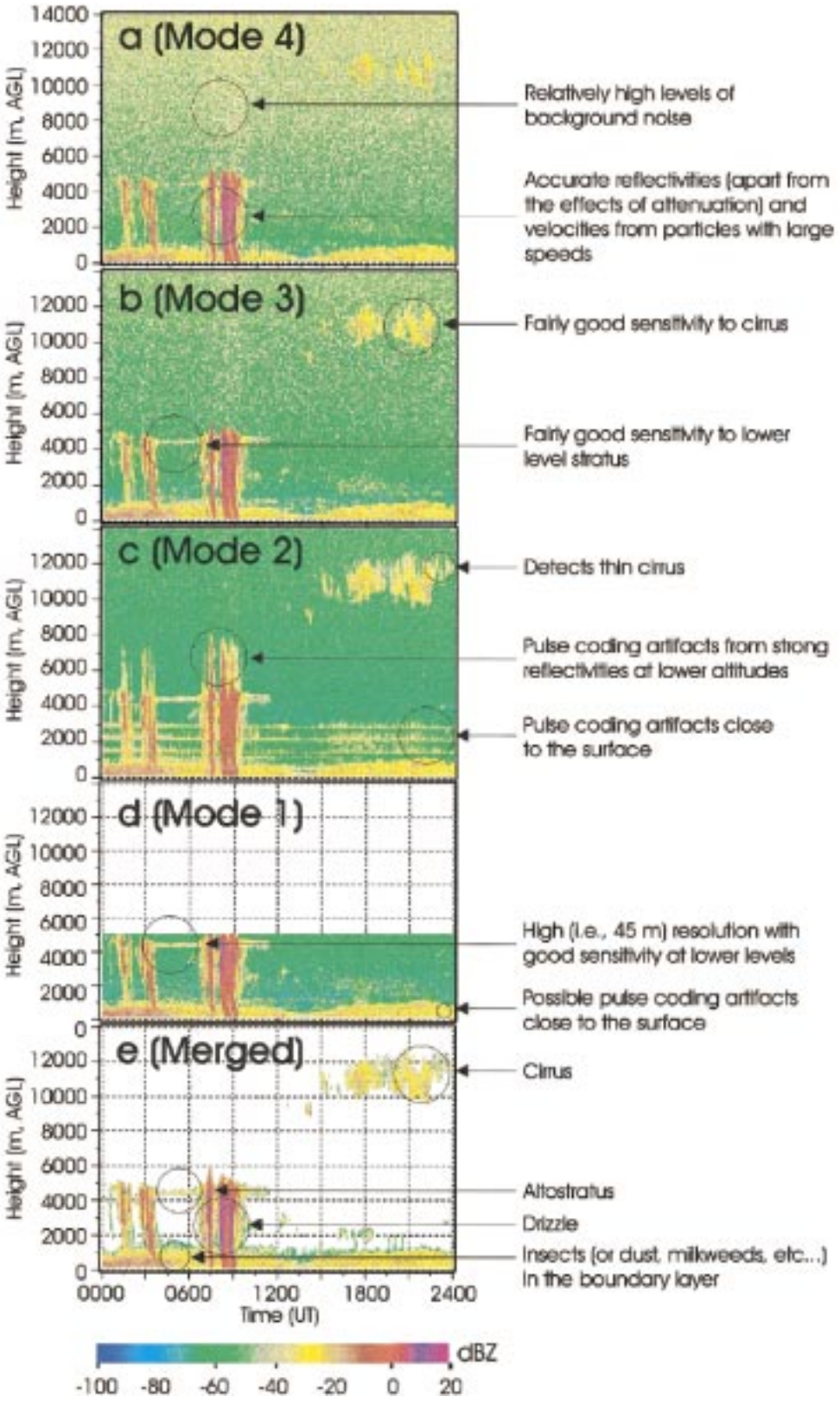

FIG. 4. Reflectivites produced by (a) SGP MMCR mode 4, (b) SGP MMCR mode 3, (c) SGP MMCR mode 2, and (d) SGP MMCR mode 1 on 21 Sep 1997. The reflectivities illustrated in (e) are obtained by first identifying the location of clouds in the data of each mode and then combining the cloud reflectivities from the four modes in such a way that any artifacts in the data from each mode are removed.

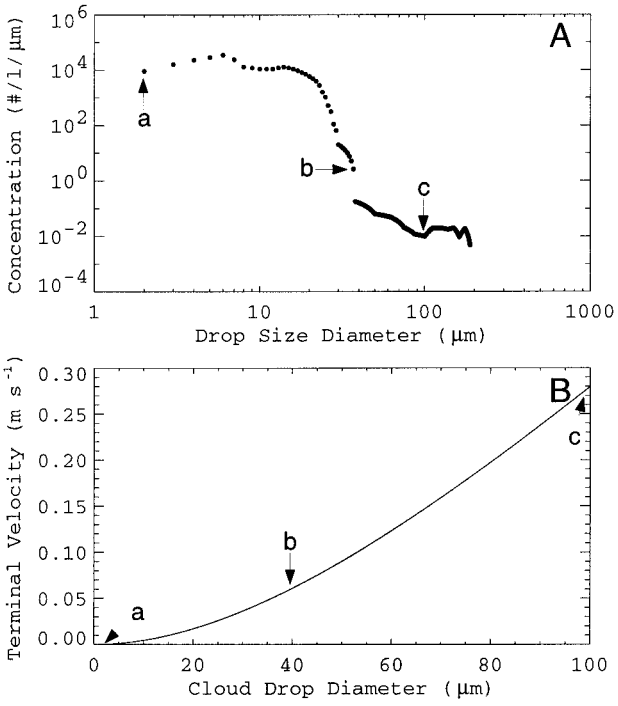

FIG. 5. (a) An example of the cloud drop concentration in units of particles L^{-1} μm^{-1} as a function of drop diameter that was obtained by cloud probes aboard the University of Wyoming King Air aircraft at Rock Springs from a stratus deck at an altitude of approximately 2.2 km. (b) Cloud drop terminal fall velocities as a function of particle diameter as presented by Rogers et al. (1993). Note that the cloud mode drops between points ''a'' and ''b'' have terminal fall velocities less than 0.09 m s^{-1} and are not resolved in the Doppler spectra produced by the current set of operational modes. However, the drizzle drops between points ''b'' and ''c'' are to an extent resolved by the current modes.

increased processor speed will mean either that more radar data can be processed during the same time interval, thus improving the overall system sensitivity for the same temporal resolution, or that the same amount of data can be processed at a much faster rate—that is, within approximately 0.5–3.0 s as opposed to 9 s—thus improving the temporal resolution without sacrificing sensitivity.

Producing spectra with more FFT points in them has an important consequence. During a recent field experiment at Rock Springs, Pennsylvania, cloud probes aboard the University of Wyoming King Air recorded the cloud drop size spectrum illustrated in Fig. 5a. Neglecting the effects of wind, the vertical velocities of the particles as a result of gravity are computed using the scheme of Rogers et al. (1993). As the results of these calculations indicate (Fig. 5b), although the drizzle particles between the points labeled ''b'' and ''c'' are resolved to an extent by the modes in current operation, the cloud mode particles between the points labeled ''a'' and ''b'' in Fig. 5a have velocities that are less than 0.09 m s^{-1} and hence fall between the 0 m s^{-1} and neighboring FFT points of all four modes currently in operation. Having a mode available with a much higher velocity resolution will allow the fall velocities of cloud particles to be resolved, which may be an important step in allowing the sizes of these particles to be retrieved from the Doppler velocity spectrum (e.g., Gossard et al. 1997).

Although power density spectra are produced routinely by the MMCRs, they can be saved only at selected times because of the large amount of memory they require. The first three moments derived from the spectra, that is, the reflectivity, the mean velocity, and the standard deviation of the velocity, are saved at full temporal resolution. Fortunately, Moran et al. (1998) configured the radar to be run remotely, so the exact sequence of modes running the radar, as well as whether or not the power density spectra are saved, can be changed quickly in order to capture interesting cloud events, using more appropriate modes.

The primary goal of the ARM 35-GHz radars, or MMCRs, is to provide a continuous record of clouds and their properties in the vertical columns above the ARM sites. Detecting the presence of clouds and cloud boundaries is the first step in ascertaining the macrophysical and microphysical properties of the clouds in the vertical column above the radar. Once the presence of clouds has been ascertained through algorithms such as those developed by Uttal et al. (1993) or Clothiaux et al. (1995), the next important step is retrieving the microphysical properties of the cloud particles, which is the subject of ongoing research by many scientific groups.

Acknowledgments. Support for this research was provided in part by the Environmental Sciences Division of the U.S. Department of Energy (under Grant DE-FG02-90ER61071) and Battelle Pacific Northwest Laboratory (Subcontract 091572-A-Q1). We would like to thank Frank Evans and Warren Wiscombe for discussions that motivated the creation of mode 1.

REFERENCES

Battan, L. J., 1973: *Radar Observation of the Atmosphere.* University of Chicago Press, 324 pp.

Clothiaux, E. E., M. A. Miller, B. A. Albrecht, T. P. Ackerman, J. Verlinde, D. M. Babb, R. M. Peters, and W. J. Syrett, 1995: An evaluation of a 94-GHz radar for remote sensing of cloud properties. *J. Atmos. Oceanic Technol.,* **12,** 201–229.

Doviak, R. J., and D. S. Zrnić, 1984: *Doppler Radar and Weather Observations.* Academic Press, 458 pp.

——, and ——, 1993: *Doppler Radar and Weather Observations.* 2d ed. Academic Press, 562 pp.

Gossard, E. E., J. B. Snider, E. E. Clothiaux, B. Martner, J. S. Gibson, R. A. Kropfli, and A. S. Frisch, 1997: The potential of 8-mm radars for remotely sensing cloud drop size distributions. *J. Atmos. Oceanic Technol.,* **14,** 76–87.

Moran, K. P., B. E. Martner, M. J. Post, R. A. Kropfli, D. C. Welsh, and K. B. Widener, 1998: An unattended cloud-profiling radar for use in climate research. *Bull. Amer. Meteor. Soc.,* **79,** 443–455.

Rogers, R. R., D. Baumgardner, S. A. Ethier, D. A. Carter, and W.

L. Ecklund, 1993: Comparison of raindrop size distributions measured by radar wind profiler and by airplane. *J. Appl. Meteor.*, **32,** 694–699.

Sauvageot, H., 1992: *Radar Meteorology.* Artech House, 366 pp.

Schmidt, G., R. Ruster, and P. Czechowsky, 1979: Complementary code and digital filtering for detection of weak VHF radar signals from the mesosphere. *IEEE Trans. Geosci. Electron.*, **17,** 154–161.

Skolnik, M. I., 1980: *Introduction to Radar Systems.* 2d ed. McGraw Hill, 581 pp.

——, 1990: *Radar Handbook.* 2d ed. McGraw Hill.

Ulaby, R. T., R. K. Moore, and A. K. Fung, 1982: *Microwave Remote Sensing: Active and Passive.* Vol. 2, *Radar Remote Sensing and Surface Scattering and Emission Theory,* Artech House, 1064 pp.

Uttal, T., L. I. Church, B. E. Martner, and J. S. Gibson, 1993: CLDSTATS: A cloud boundary detection algorithm for vertically pointing radar data. NOAA Tech. Memo. ERL WPL-233, Environmental Technology Laboratory, Boulder, Colorado, 28 pp. [Available from National Technical Information Service, 5285 Port Royal Rd., Springfield, VA 22161.]

Wakasugi, K., and S. Fukao, 1985: Sidelobe properties of a complementary code used in MST radar observations. *IEEE Trans. Geosci. Remote Sens.*, **GE-23,** 57–59.